Dalton Transactions

RSC Publishing

PAPER

View Article Online
View Journal | View Issue

Cite this: *Dalton Trans.*, 2013, **42**, 8347

Copper(II) complexes with 2NO and 3N donor ligands: synthesis, structures and chemical nuclease and anticancer activities†

Chandrasekaran Rajarajeswari,[a] Rangasamy Loganathan,[b] Mallayan Palaniandavar,*[b] Eringathodi Suresh,[c] Anvarbatcha Riyasdeen[d] and Mohamad Abdulkadhar Akbarsha[e,f]

Received 13th December 2012,
Accepted 2nd April 2013

DOI: 10.1039/c3dt32992e

www.rsc.org/dalton

A series of water soluble copper(II) complexes of the types [Cu(L)Cl] **1–2**, where LH is 2-(2-(1*H*-benzimidazol-2-yl)ethyliminomethyl)phenol (H(**L1**)), and 2-(2-(1*H*-benzimidazol-2-yl)-ethyliminomethyl)-4-methylphenol (H(**L2**)), and [Cu(L)Cl_2] **3**–**6**, where L is (2-pyridin-2-yl-ethyl)pyridin-2-ylmethyleneamine (**L3**), 2-(1*H*-benzimidazol-2-yl)ethylpyridin-2-yl-methyleneamine (**L4**), 2-(1*H*-benzimidazol-2-yl)ethyl(1*H*-imidazol-2-ylmethylene)amine (**L5**), and 2-(1*H*-benzimidazol-2-yl)ethyl-(4,4a-dihydroquinolin-2-ylmethylene)amine (**L6**), have been isolated and characterized by elemental analysis, electronic absorption, ESI-MS and EPR spectral techniques and the electrochemical method. The single crystal X-ray structures of [Cu(L1)Cl] **1** and [Cu(L2)Cl] **2** possess a distorted square-based coordination geometry while [Cu(L4)Cl_2] **4** and [Cu(L6)Cl_2] **6** possess a distorted trigonal bipyramidal coordination geometry. Both absorption spectral titration and an EthBr displacement assay reveal that all the complexes bind with calf thymus (CT) DNA through covalent mode of DNA interaction involving the replacement of an easily removable chloride ion with DNA nucleobases. All the complexes exhibit oxidative cleavage of supercoiled (SC) plasmid DNA in the presence of hydrogen peroxide as an activator. It is remarkable that at 50 μM concentration **5** and **6** completely degrade SC DNA into undetectable minor fragments and thus they act as efficient chemical nucleases. All the complexes are remarkable in displaying cytotoxicity against the HBL-100 human breast cancer cell line with potency more than that of the widely used drug cisplatin and hence they have the potential to act as promising anticancer drugs. Interestingly, they are non-toxic to normal cell lymphocytes isolated from human blood samples, revealing that they are selective in killing only the cancer cells.

Introduction

Inorganic chemistry offers wide scope for the design of novel drugs based on the coordination and redox properties of metal compounds[1] and studies on metal based drugs offer promise in the fight against cancer.[2,3] The exploration of medicinal applications of metal-based anticancer drugs is driven by the necessity to fill the gap in tumor chemotherapy, which includes minimization of undesirable side-effects, overcoming the resistance problem, and enlarging the spectrum of activity to more tumor types and to metastatic cancers. The routes toward rational drug design are provided by studying the interaction of these small molecules with DNA and also their reaction at specific sites along a DNA strand as reactive models for protein–nucleic acid interactions. A good number of metal complexes have been used as agents for mediation of strand scission of duplex DNA and thus act as chemotherapeutic

[a]*School of Chemistry, Bharathidasan University, Tiruchirappalli – 620 024, Tamil Nadu, India*
[b]*Department of Chemistry, Central University of Tamil Nadu, Thiruvarur 610004, Tamil Nadu, India. E-mail: palanim51@yahoo.com, palaniandavarm@gmail.com*
[c]*Analytical Science Discipline, Central Salt and Marine Chemical Research Institute, Bhavnagar 364 002, India*
[d]*Department of Animal Science, Bharathidasan University, Tiruchirappalli – 620 024, Tamil Nadu, India*
[e]*Mahatma Gandhi-Doerenkamp Center for Alternatives to use of Animals in Life Science Education, Bharathidasan University, Tiruchirappalli, 620024, Tamil Nadu, India*
[f]*Department of Food Sciences and Nutrition, College of Food Sciences and Agriculture, King Saud University, Riyadh-11451, Kingdom of Saudi Arabia*
†Electronic supplementary information (ESI) available. CCDC 814241–814244. For ESI and crystallographic data in CIF or other electronic format see DOI: 10.1039/c3dt32992e

agents.[4–9] Over the past decade the development of new metal-based reagents for biotechnology has been the subject of intense investigation and many potential redox and spectroscopically active Cu(II/I) and Ru(II/III) complexes have been designed as new chemical nucleases[10,11] and their DNA binding properties studied.[12–14] Sigman and his co-workers[15,16] have shown that the cationic complex $[Cu(phen)_2]^+$, where phen is 1,10-phenanthroline, in the presence of molecular oxygen and a reducing agent, acts as an efficient nuclease by oxidative cleavage with a high preference for double-strand DNA. Several other copper-based synthetic nucleases have been reported[17–19] and there are a few reports of copper complexes cleaving DNA hydrolytically.[20,21] Over the past several years there has been continuous interest in determining the mode and extent of binding of metal complexes to DNA, as such information is important for understanding the cleavage properties of metal complexes, and hence for developing cleaving agents for probing nucleic acid structures and for other applications.

Metal complexes are known to bind to DNA *via* both covalent and non-covalent interactions. In covalent binding the labile ligand of the complexes is replaced by a nitrogen base of DNA such as guanine N7. Only limited reports on the covalent interaction of metal complexes with DNA are available. Cisplatin, an important antitumor drug, is thought to bind to DNA through an intrastrand crosslink between neighboring guanine residues created by covalent binding to two soft purine nitrogen atoms. The complex $[Ru(phen)_2Cl_2]$ binds covalently to DNA duplex and exhibits striking enantiomeric selectivity different from that seen upon intercalation.[22] In our laboratory, we have studied the covalent mode of DNA binding of $[Cu(L)Cl_2]$ complexes derived from linear 3N ligands.[23] In contrast to the covalent mode of DNA interaction, the non-covalent mode of DNA interaction includes intercalation, which involves partial insertion of aromatic heterocyclic rings of ligands between the DNA base pairs, and electrostatic and groove (surface) binding, which involves binding of cationic metal complexes along the outside of the DNA helix, along the major or minor groove. In our laboratory, we have focused our attention also on various non-covalent DNA interactions of redox-active Cu(II),[24–27] Ru(II)[28,29] and Co(III)[30] complexes. We have very recently reported several mixed ligand copper(II) complexes with tri- and tetradentate primary ligands and a series of simple and substituted phen as co-ligands, which act as recognition elements in non-covalent DNA interaction.[31–37] Many of these complexes bind and cleave DNA and show promising chemotherapeutic activity more potent than cisplatin, which correlates well with their strong DNA binding affinity. So, studies on interaction of copper(II) complexes with DNA are useful in the rational design of small molecule anticancer therapeutics.

The present work stems from our continued interest in defining and evaluating the key DNA-binding interactions of copper(II) complexes of pyridine and benzimidazole based ligands and also from our efforts to explore the relationship between the structure and nuclease activity of metal complexes of polypyridine ligands,[26,28,29] which would ultimately help in the design of newer drugs and also develop useful DNA structural probes and new selective and efficient DNA recognition and cleaving agents. As the exact mode and extent of DNA binding and DNA cleaving mechanisms of the covalently DNA binding complexes remain unclear, and are expected to exhibit more potent DNA binding affinity, we have synthesized a series of new coordinatively unsaturated copper(II) complexes of the types [Cu(L)Cl], where LH is a tridentate Schiff base ligand derived from the condensation of salicylaldehyde (H(**L1**)), 5-methylsalicylaldehyde (H(**L2**)), and $[Cu(L)Cl_2]$, where L is a tridentate Schiff base ligand derived from condensation of pyridine-2-carboxaldehyde with 2-aminoethylpyridine (**L3**), and that of pyridine-2-carboxaldehyde (**L4**), imidazole-2-carboxaldehyde (**L5**) and quinoline-2-carboxaldehyde (**L6**) with aminoethylbenzimidazole, and intend to explore the binding properties of the complexes with calf thymus (CT) DNA using a host of physical methods like absorption and fluorescence spectroscopy and gel electrophoresis.

The complexes isolated are square-planar with one or two labile chloride ions, which may be replaced upon covalent binding with guanine N7 of DNA and the benzimidazole (bzim)/quinolyl ligand moiety may act as a DNA recognition element by involving in non-covalent interaction with DNA. The bzim scaffold has been shown to be a useful structural motif for the development of molecules of pharmaceutical and/or biological interest.[38] Benzimidazole derivatives are important pharmacophores in drugs that display diverse pharmacological activities, such as anti-inflammatory, antioxidant, gastroprotective and antiparasitic activities.[39] Appropriately substituted bzim derivatives have found diverse therapeutic applications as antiulcers, antihypertensives, antiviral, antifungals, anticancer, and antihistaminics.[39] The optimization of bzim-based structures has resulted in various drugs that are currently on the market, such as omeprazole, pimobendan and mebendazole.[38] Also, we have now shown that mixed ligand copper(II) complexes of *N*,*N*′-bis(benzimidazol-2-ylmethyl)-amine (bba) exhibit double-strand DNA cleavage and protein cleavage activities and display remarkable cytotoxicity against SiHa cervical cancer cell lines by generating ROS species leading to induction of apoptosis followed by cell death.[31] The X-ray structures of four of the present complexes have been successfully determined to assess the effect of varying the ligand steric bulk and hydrophobicity exhibited by pyridyl, bzim, imidazolyl and quinolyl groups on the coordination geometry and hence explore the DNA binding structure and cleavage activity of the complexes. Interestingly, the present complexes of tridentate ligands with labile chloride ions are involved in strong covalent binding with DNA and display moderate DNA cleavage activity but significant anticancer activities.

Experimental section

Materials

Copper(II) chloride dihydrate (Merck, India), salicylaldehyde (Merck, India), 5-methyl-salicylaldehyde (Aldrich), pyridine-2-

carboxaldehyde (Aldrich), imidazole-2-carboxaldehyde (Aldrich), quinoline-2-carboxaldehyde (Aldrich), 2-aminoethylpyridine (Aldrich), β-alanine (Sigma) and 1,2-phenylenediamine (SISCO) were used as received. A series of ligands H(**L1**), H(**L2**) and **L3–L6** was synthesized by using reported procedures.[41–44] The commercial solvents were distilled and then used for the preparation of ligands and complexes. The supporting electrolyte tetra-*n*-butylammonium perchlorate (TBAP) was prepared in water and recrystallized twice from aqueous ethanol. Disodium salt of calf thymus DNA (highly polymerized) purchased from Sigma was stored at 4 °C and used as received. The supercoiled pUC19 plasmid DNA was purchased from Genei, Bangalore. Ultra-pure MilliQ water (18.2 μΩ) was used in all experiments. Solutions of DNA in buffer, 50 mM NaCl/5 mM Tris-HCl in water, gave a ratio of UV absorbance at 260 and 280 nm, A_{260}/A_{280}, of 1.9, which indicated that the DNA was sufficiently free of protein.[40] Concentrated stock solutions of DNA were prepared in buffer and sonicated for 25 cycles, where each cycle consisted of 30 s with 1 min intervals. The concentration of DNA in nucleotide phosphate (NP) was determined by UV absorbance around 260 nm after 1 : 100 dilutions by taking the extinction coefficient, ε_{260}, as 6600 M^{-1} cm^{-1}. Stock solutions were stored at 4 °C and used after not more than 4 days.

Cell culture

The human breast cancer cell line (HBL-100) was obtained from the National Center for Cell Science (NCCS), Pune, India. The cells were cultured in RPMI 1640 medium (Biochrom AG, Berlin, Germany) supplemented with 10% fetal bovine serum (Sigma), cisplatin (Getwell Pharmaceuticals, India), mitomycin C (Sigma) and 100 U ml^{-1} penicillin and 100 μg ml^{-1} streptomycin as antibiotics (Himedia, Mumbai, India) in 96-well culture plates at 37 °C under a humidified atmosphere of 5% CO_2 in a CO_2 incubator (Heraeus, Hanau, Germany). All experiments were performed using cells from passage 15 or less.

Methods and measurements

Crystallographic refinements and structure solution

A crystal of suitable size selected from the mother liquor was immersed in paraffin oil, mounted on the tip of a glass fiber and then cemented using epoxy resin. Intensity data for the crystals were collected using Mo Kα (λ = 0.71073) radiation on a Bruker SMART APEX diffractometer equipped with a CCD area detector at 293 and 296 K. The crystallographic data were collected in Table 1. The *SMART*[45] program was used for collecting frames of data, indexing the reflections, and determination of lattice parameters; the *SAINT*[45] program for integration of the intensity of reflections and scaling; the *SADABS*[46] program for absorption correction, and the *SHELXTL*[47] program for space group and structure determination and least-squares refinements on F^2. The structure was solved by the heavy-atom method. Other non-hydrogen atoms were located in successive difference Fourier syntheses. The final refinement was performed by full-matrix least-squares analysis. Hydrogen atoms attached to the moiety were located from the difference Fourier map and refined isotropically.

Electrochemical measurements

All cyclic voltammetry (CV) experiments were performed in a single compartment cell with a three electrode configuration on an EG & G PAR 273 potentiostat/galvanostat equipped with a Pentium IV computer, along with EG & G M270 software to carry out the experiments and to acquire the data. A platinum sphere, a platinum plate, and Ag/Ag^+ were used as working, auxiliary, and reference electrodes, respectively. TBAP was used as a supporting electrolyte (100 mM). Solutions were deoxygenated by purging with nitrogen gas for 15 min prior to the measurements. All the measurements were carried out at 25 ± 0.2 °C, maintained by a cryocirculator (HAAKE D8-G). The redox potential ($E_{1/2}$) was calculated from the anodic (E_{pa}) and

Table 1 Crystal data and structure refinement for [Cu(L1)Cl] **1**, [Cu(L2)Cl] **2**, [$Cu(L4)Cl_2$] **4** and [$Cu(L6)Cl_2$] **6**

	1	**2**	**4**	**6**
Empirical formula	$CuC_{16}H_{14}N_3OCl.CH_3CN$	$CuC_{17}H_{15}N_3OCl.H_2O$	$CuC_{15}H_{14}N_4Cl_2$	$CuC_{19}H_{16}N_4Cl_2.CH_3OH.H_2O$
Fw	404.35	395.99	384.75	484.86
Crystal syst	Triclinic	Monoclinic	Orthorhombic	Monoclinic
Space group	$P\bar{1}$	$P2_1/c$	$P2_12_12_1$	$P2(1)/n$
a (Å)	8.1634(10)	7.087(3)	8.657(2)	10.3104(5)
b (Å)	10.2365(13)	15.617(7)	12.581(3)	17.1202(9)
c (Å)	11.6844(15)	15.156(7)	14.030(4)	11.9361(6)
α (°)	108.091(2)	90	90	90
β (°)	108.147(2)	101.024(8)	90	90.781(3)
γ (°)	92.647(2)	90	90	90
V ($Å^3$)	870.86(19)	1646.5(13)	1528.1(7)	2106.72(18)
Z	2	4	4	4
ρ calcd (g cm^{-3})	1.542	1.591	1.672	1.529
F (000)	414	808	780	996
T (K)	100(2)K	293(2)K	296(2)K	296(2)K
Radiation [Mo Kα] (Å)	0.71073	0.71073	0.71073	0.71073
Residuals [$I > 2\sigma(I)$]				
$R1$[a]	0.0560	0.0786	0.0627	0.0391
w$R2$[b]	0.1120	0.1835	0.1415	0.0877

[a] $R1 = [\Sigma(||F_o| - |F_c||)/\Sigma|F_o|]$. [b] $wR2 = \{[\Sigma(w(F_o^2 - F_c^2)^2)/\Sigma(wF_o^4)]^{1/2}\}$.

cathodic (E_{pc}) peak potentials of CV traces as (E_{pa} + E_{pc})/2. The redox potentials were estimated from the DPV (differential pulse voltammetry) peak potential, E_p, using the relation $E_{1/2}$ = E_p + $\Delta E/2$, where $E_{1/2}$ is the equivalent of the average of E_{pa} and E_{pc} in CV experiments and ΔE is the pulse amplitude.

Electron paramagnetic resonance spectral measurements

EPR spectra of the complexes in methanol at liquid nitrogen temperature (77 K) were recorded on a JEOL JES-TE100 ESR spectrometer operating at X-band frequencies and having a 100 kHz field. DPPH was used as the field marker.

DNA binding and DNA cleavage studies

Absorption spectra were recorded on a UV-2450 Shimadzu spectrophotometer using cuvettes of 1 cm path length. For absorption and emission spectral experiments the DNA solutions were pretreated with the solutions of metal complexes to ensure no change in the metal complex concentrations. Absorption spectral titration experiments were performed by maintaining a constant concentration of the complex and varying the DNA concentration. This was achieved by dissolving an appropriate amount of the metal complex and DNA stock solutions while maintaining the total volume constant (1 ml). This results in a series of solutions with varying concentrations of DNA but with a constant complex concentration. The absorption (A) was recorded after successive additions of CT DNA. The intense ligand based (π–π^*) absorption band of the complexes was used to monitor the interaction of the complexes with CT DNA. Emission intensity measurement was carried out using a JASCO F 6500 spectrofluorimeter. The Tris buffer was used as a blank to make preliminary adjustments. The excitation wavelength was fixed and the emission range was adjusted before measurements. DNA was pretreated with ethidium bromide in the ratio [DNA]/[EthBr] = 10 for 30 min at 27 °C. The metal complexes were then added to this mixture and their effect on the emission intensity was measured.

The supercoiled pUC19 DNA cleavage with added reductant hydrogen peroxide was monitored using agarose gel electrophoresis. Reactions using supercoiled pUC19 plasmid DNA (Form I, 40 μM, in base pairs) in a 5 mM Tris-HCl and 50 mM NaCl buffer at pH 7.1 were treated with metal complex (30 μM) and hydrogen peroxide (100 μM), followed by dilution with the Tris-HCl buffer to a total volume of 20 μL. The samples were incubated for 1 h at 37 °C. A loading buffer containing 25% bromophenol blue, 0.25% xylene cyanol, and 30% glycerol (3 μL) was added, and electrophoresis was performed at 60 V for 5 h in Tris-acetate–EDTA (TAE) buffer (40 mM Tris base, 20 mM acetic acid, 1 mM EDTA) using 1% agarose gel containing 1.0 μg ml^{-1} EthBr. The gel was viewed in an Alpha Innotech Corporation Gel doc system and photographed using a CCD camera. Densitometric calculations were made using the Alpha Ease FC Stand Alone software. The intensities of supercoiled DNA were corrected by a factor of 1.47 as a result of its lower staining capacity by EthBr.[48] The cleavage efficiency was measured by determining the ability of the complex to convert supercoiled DNA (SC) to nicked circular form (NC) and linear form (LC).

MTT assay

An MTT assay was carried out as described previously.[49] The complexes in the concentration range of 0.05–50 μg ml^{-1}, dissolved in DMSO (Sigma-Aldrich, St. Louis, MO, USA), were added to the wells 24 h after seeding of 5×10^3 cells per well in 200 μl of fresh culture medium. DMSO was used as the vehicle control. After 24 and 48 h, 20 μl of MTT solution [5 mg ml^{-1} in phosphate-buffered saline (PBS)] was added to each well and the plates were wrapped with aluminum foil and incubated for 4 h at 37 °C. The purple formazan product formed was dissolved by addition of 100 μl of 100% DMSO to each well. The absorbance was monitored at 570 nm (measurement) and 630 nm (reference) using a 96 well plate reader (Bio-Rad, Hercules, CA, USA). The stock solutions of the metal complexes were prepared in DMSO and in all the experiments the percentage of DMSO was maintained in the range of 0.1–1%. DMSO by itself was found to be non-toxic to the cells till 1% concentration. Data were collected for four replicates each and were used to calculate the mean. The percentage inhibition was calculated from these data using the formula:

$$= \frac{\text{Mean OD of untreated cells (control)} - \text{Mean OD of treated cells}}{\text{Mean OD of untreated cells (control)}} \times 100$$

The IC_{50} values were calculated using *Table Curve 2D*, version 5.01.

Lymphocyte isolation and lymphocyte cytotoxicity assay

Five ml of venous blood was collected and defibrinated by using glass beads. Two ml of lymphoprep solution (Biotest, Germany) was transferred to a clean, sterile serology tube and 4 ml of diluted blood (diluted with an equal volume of saline) was gently overlaid onto the lymphoprep solution (do not mix the blood–lymphoprep solution). The tubes were spun at 1600 rpm for 20 minutes. After centrifugation the interphase layer (white buffy-coat) containing the lymphocyte was carefully scooped out using a glass Pasteur pipette and transferred to another serology tube. The lymphocytes were washed twice in saline and packed at 1500 rpm for 10 minutes. The final pellet was adjusted to a concentration of 4×10^6 cells ml^{-1} in saline.

Complexes **1–6** were tested with a microlymphocytotoxicity assay for cell viability counting (Terasaki and McClelland, 1964). The complexes in the concentration range of 10–100 μM were added to a 72 well Terasaki microtitre plate which consists of 12 columns (**1–6**) and 12 rows (A–F) having 2 μl of lymphocyte suspension. In each row, one positive (ALS, anti-lymphocyte serum, Biotest, Germany) and one negative control (saline) well was maintained. Compounds **1–6** were serially diluted as 1×, 1 : 2, 1 : 4, and 1 : 8. Two μl of each dilution of each compound was added to the respective wells. One row for each compound was used for the assay. After the dilutions

were made the plates were kept in RT for half an hour. After 30 minutes of incubation, 5 μl of a fluorescent dye mixture of acridine orange and EthBr (AOEB) was added to all the wells. After 5 minutes, 5 μl of formaldehyde was added in order to stop the reaction followed by 5 μl of packed RBCs for quenching the excess fluorescence. The results were observed and documented by a 20× phase contrast microscope (Nikon, Japan). Typing trays were scored manually taking into consideration the number of dead cells compared to the cells in the positive control well (ALS) and the negative control well.

Results and discussion

Synthesis of ligands and complexes

A series of ligands H(**L1**), H(**L2**), **L3–L6** was synthesized by condensing 2-amino-ethylbenzimidazole/aminoethylpyridine with the corresponding aldehydes to form Schiff bases (Scheme 1). The copper(II) complexes of the ligands were prepared by the reaction between copper(II) chloride dihydrate and the corresponding ligands in equimolar quantities using methanol and acetonitrile as solvents. Complexes **3** and **5** were isolated as green colored powders while the others as green crystals. The formulae of the complexes [Cu(L)Cl] **1–2** and [Cu(L)Cl_2] **3–6**, as determined by elemental analysis, are supported by the X-ray crystal structures of **1**, **2**, **4** and **6** (*cf.* below). A systematic variation in the aromatic donor moiety of the 3N and 2NO ligands is expected to significantly tune the molecular structures and electronic properties of the complexes and so the complexes are expected to show variation in DNA binding affinity, DNA cleavage ability and anticancer activity.

Description of the crystal structures of 1, 2, 4 and 6

Structure of [Cu(L1)Cl]·CH_3CN 1. The ORTEP representation of the structure of [Cu(L1)Cl] **1** including the atom numbering scheme is shown in Fig. 1. The crystal structure refinement data are provided in Table 1 and the selected bond lengths and bond angles are given in Table 2. The asymmetric unit of the compound contains one complex molecule and one lattice acetonitrile solvent molecule. The copper(II) centre is in a square-based (2NOCl) coordination environment constituted by the phenolate oxygen (O1), bzim nitrogen (N2) and imine nitrogen (N1) of the deprotonated ligand and the chloride ion (Cl1). Both the nitrogen atoms and the oxygen atom of the meridionally coordinated ligand occupy three corners of the square plane with the chloride ion located at the fourth corner. The copper(II) is located above the O1N1N2Cl1 plane as indicated by the values of the diagonal angles O1–Cu1–N2 (150.84°) and N1–Cu1–Cl1 (140.88°), which deviate from the ideal angle of 180°.[50] The sum (Σ) of the six inter-bond angles[51] for **1** is 671°, which deviates from the ideal angle of 720°, suggesting that the geometry around copper(II) is distorted square planar. Also, the *cis* angles in the basal plane involving the phenolate oxygen and imine nitrogen (O1–Cu1–N1, 93.28°) and that involving imine nitrogen and bzim nitrogen (N1–Cu(1)–N2, 92.60°) deviate from the ideal value of 90°, suggesting that the square planar coordination geometry in **1** is slightly distorted due to the chelate effect. The Cu–N_{imine} (Cu1–N1, 1.951(3) Å) and Cu–N_{bzim} bond lengths (Cu1–N2, 1.977(3) Å) are similar to those reported for other square-based Cu(II) complexes containing similar ligands (Cu–N_{imine}, 1.936–1.955 Å; Cu–N_{bzim}, 1.992–2.0511 Å).[51–58] .The Cu–Cl1 bond [2.2474(11) Å)] is similar to those reported for copper(II) chloride complexes (2.2347–2.2480 Å).[54–56,59,60] The Cu–$O_{phenolate}$ bond length (1.908(3) Å) is comparable with those (Cu–O, 1.912(5) Å) in the analogous complex [Cu(L)Cl], where HL is *N*-(2-pyridylmethyl)-3-methoxysalicylaldimine,[53] and is similar to those reported for other square-planar Cu(II) complexes containing similar ligands (Cu–O, 1.917–1.929 Å).[54–56]

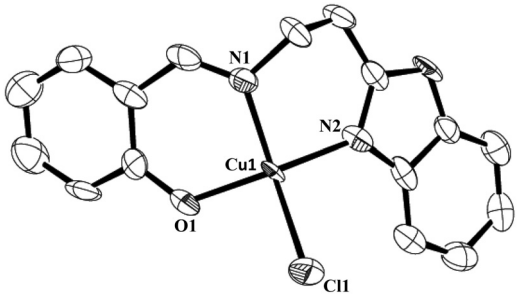

Fig. 1 ORTEP diagram of **1** showing 45% probability thermal ellipsoids and the labeling scheme for selected atoms. All of the hydrogen atoms are omitted for clarity.

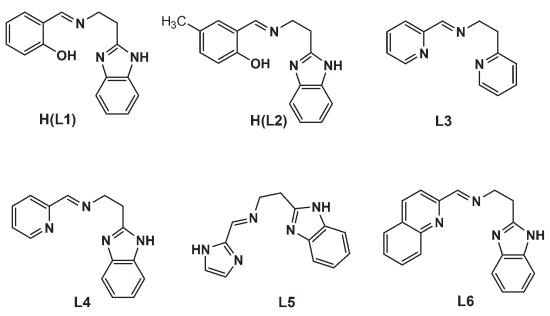

Scheme 1 Structures of tridentate ligands H(**L1**), H(**L2**) and **L3–L6**.

Structure of [Cu(L2)Cl]·H_2O 2. The ORTEP representation of the structure of [Cu(L2)Cl] **2** including the atom numbering scheme is shown in Fig. 2. The crystal structure refinement data are provided in Table 1 and the selected bond lengths and bond angles are collected in Table 2. The asymmetric unit cell of [Cu(L2)Cl] contains one complex molecule and one water molecule. The copper(II) center is in a square-based planar (2NOCl) coordination environment constituted by the phenolate oxygen (O1), bzim nitrogen (N3) and imine nitrogen (N1) of the deprotonated ligand and the chloride ion (Cl1). The copper atom is located above the O1N1N3Cl1 plane as indicated by the diagonal angles O1–Cu1–N3 (142.6°) and N1–Cu1–Cl1 (143.27°). The sum (Σ) of the six inter-bond angles[51] for **2** is 669°, which deviates from the ideal angle of 720°, suggesting that the geometry around copper(II) is distorted

Table 2 Selected bond lengths [Å] and bond angels [°] for [Cu(L1)Cl] **1**, [Cu(L2)Cl] **2**, [Cu(L4)Cl_2] **4** and [Cu(L6)Cl_2] **6**

1		**2**		**4**		**6**	
Cu(1)–O(1)	1.908(3)	Cu(1)–O(1)	1.892(4)	Cu(1)–N(1)	2.055(5)	Cu(1)–N(1)	2.041(2)
Cu(1)–N(1)	1.951(3)	Cu(1)–N(1)	1.926(5)	Cu(1)–N(2)	2.023(5)	Cu(1)–N(2)	2.050(2)
Cu(1)–N(2)	1.977(3)	Cu(1)–N(3)	1.983(5)	Cu(1)–N(3)	2.019(5)	Cu(1)–N(3)	1.972(2)
Cu(1)–Cl(1)	2.2474(11)	Cu(1)–Cl(1)	2.2440(19)	Cu(1)–Cl(1)	2.4928(18)	Cu(1)–Cl(1)	2.360(8)
				Cu(1)–Cl(2)	2.270(17)	Cu(1)–Cl(2)	2.3541(7)
O(1)–Cu(1)–N(1)	93.28(13)	O(1)–Cu(1)–N(1)	95.00(2)	N(3)–Cu(1)–N(1)	162.1(2)	N(3)–Cu(1)–N(1)	169.19(9)
O(1)–Cu(1)–N(2)	150.84(13)	O(1)–Cu(1)–N(3)	142.6(2)	N(3)–Cu(1)–N(2)	90.7(2)	N(3)–Cu(1)–N(2)	90.23(9)
N(1)–Cu(1)–N(2)	92.60(13)	N(1)–Cu(1)–N(3)	92.50(2)	N(2)–Cu(1)–N(1)	78.6(2)	N(1)–Cu(1)–N(2)	79.61(9)
O(1)–Cu(1)–Cl(1)	93.04(9)	O(1)–Cu(1)–Cl(1)	94.82(15)	N(3)–Cu(1)–Cl(2)	94.94(15)	N(3)–Cu(1)–Cl(2)	94.70(6)
N(1)–Cu(1)–Cl(1)	140.88(11)	N(1)–Cu(1)–Cl(1)	143.27(16)	N(2)–Cu(1)–Cl(2)	156.00(18)	N(1)–Cu(1)–Cl(2)	92.87(6)
N(2)–Cu(1)–Cl(1)	100.19(10)	N(3)–Cu(1)–Cl(1)	100.79(15)	N(1)–Cu(1)–Cl(2)	89.59(16)	N(2)–Cu(1)–Cl(2)	114.24(7)
				N(3)–Cu(1)–Cl(1)	104.09(16)	N(3)–Cu(1)–Cl(1)	91.79(6)
				N(2)–Cu(1)–Cl(1)	98.30(18)	N(3)–Cu(1)–Cl(1)	90.08(6)
				N(1)–Cu(1)–Cl(1)	91.66(15)	N(2)–Cu(1)–Cl(1)	119.81(7)
				Cl(2)–Cu(1)–Cl(1)	102.89(7)	Cl(2)–Cu(1)–Cl(1)	125.48(3)

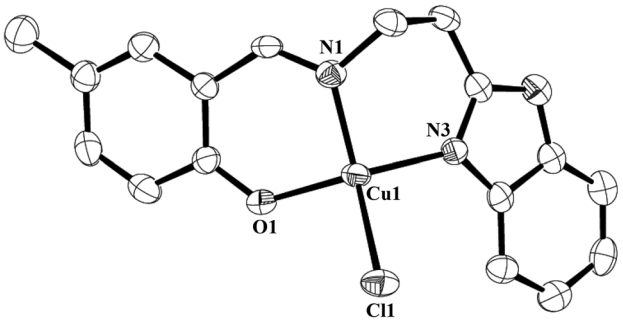

Fig. 2 ORTEP diagram of **2** showing 40% probability thermal ellipsoids and the labeling scheme for selected atoms. All of the hydrogen atoms are omitted for clarity.

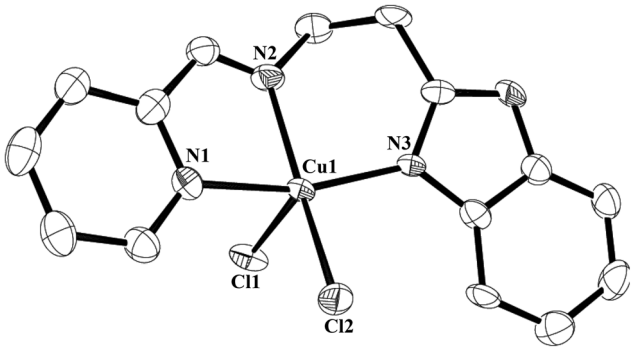

Fig. 3 ORTEP diagram of **4** showing 45% probability thermal ellipsoids and the labeling scheme for selected atoms. All of the hydrogen atoms are omitted for clarity.

square planar. The *cis* angles in the basal plane involving the phenolate oxygen and imine nitrogen are (O1–Cu1–N1, 95.00°), and that involving imine nitrogen and bzim nitrogen (N1–Cu(1)–N2, 92.50°) show deviation from the ideal value of 90°, suggesting that the square planar coordination geometry in **2** is slightly distorted due to chelate effect. On incorporating the methyl group on the salicylaldehyde moiety in **1** to obtain **2**, the Cu–$O_{phenolate}$ bond becomes shorter obviously due to the electron-releasing effect of the methyl group. The coordination geometry around Cu(II) in **2** is similar to that in **1** and the Cu–N_{imine} (Cu1–N1, 1.926(5) Å), Cu–N_{bzim} (Cu1–N3, 1.983(5) Å) and Cu–Cl1 (2.2440(19) Å) bond lengths are similar to those in **1**.

Structure of [Cu(L4)Cl_2] 4. The ORTEP representation of the structure of [Cu(L4)Cl_2] **4** including the atom numbering scheme is shown in Fig. 3. The crystal structure refinement data are provided in Table 1 and the selected bond lengths and bond angles are given in Table 2. The asymmetric unit cell of **4** contains one complex molecule in which the copper(II) is coordinated to all the three nitrogen atoms of the tridentate ligand L4 and two chloride ions as well. The coordination geometry around Cu(II) can be best described as trigonal bipyramidal distorted square based pyramidal (TBDSBP) as indicated by the value of the trigonal index τ of 0.10 ($\tau = (\alpha - \beta)/60$, where α = 162.01° and β = 155.98°; τ is 1 for a perfect trigonal bipyramidal geometry and is zero for a perfect square pyramidal geometry).[61] All the three nitrogen atoms (N1, N2, N3) of the meridionally coordinated 3N ligand occupy the three corners of the square plane, the chloride ion (Cl1) occupies the remaining corner and the other chloride ion (Cl2) occupies the axial position. The Cu–N_{py} (2.055(5) Å), Cu–N_{imine} (2.023(5) Å), and Cu–N_{bzim} (2.019(5) Å) bond distances fall in the ranges expected for similar Cu(II) complexes.[31,53] The Cu–N_{py} (2.055(5) Å) bond is longer than the Cu–N_{bzim} bond suggesting the stronger coordination of the bzim nitrogen, which is as expected (pK_a: pyH^+, 5.14; $bzimH^+$, 5.40).[62] The axial Cu–Cl1 bond (2.4928(18) Å) is longer than the equatorial Cu–Cl2 bond (2.270(17) Å), obviously because the $d_{x^2-y^2}$ orbital in a Cu(II) square pyramidal geometry contains two electrons while the d_{z^2} orbital only one electron. The two Cu–Cl bond distances are comparable to those (2.302(1), 2.538(1) Å) found in the related CuN_3Cl_2 complex[63,64] in which the Cu(II) ion adopts a similar geometry.

Structure of [Cu(L6)Cl_2]·CH_3OH·H_2O 6. The ORTEP representation of the structure of [Cu(L6)Cl_2] **6** including the atom numbering scheme is shown in Fig. 4. The crystal structure refinement data are provided in Table 1 and the selected

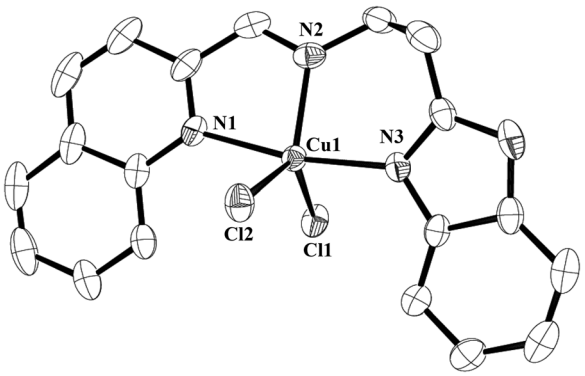

Fig. 4 ORTEP diagram of **6** showing 30% probability thermal ellipsoids and the labeling scheme for selected atoms. All of the hydrogen atoms are omitted for clarity.

bond lengths and bond angles are given in Table 2. The asymmetric unit cell of the compound contains one complex molecule and water and a methanol molecule. The copper(II) in the complex is coordinated to three nitrogen atoms, that from quinolyl, bzim moieties and that from the imine function of the tridentate ligand **L6** and two chloride ions. The coordination geometry around copper(II) can be best described as a distorted trigonal bipyramidal square based pyramidal (SBPDTB) geometry, as indicated by the value of the trigonal index τ of 0.82. One of the nitrogen atoms (N_{imine}) and two chloride ions occupy the basal positions and Cu–N_{quin} and Cu–N_{bzim} occupy the axial positions in the trigonal bipyramidal square based geometry. Interestingly, the τ values indicate that the replacement of the pyridyl moiety in **4** with a TBDSBP geometry by the bulky quinolyl moiety to give **6** enhances the steric constraints around copper(II) and confers the SBPDTB geometry. The Cu–N_{imine} (2.050 (2) Å) bond is longer than the Cu–N_{bzim} bond (1.972(2) Å), as expected (*cf.* above), and is slightly longer than the Cu–N_{quin} bond (2.041(2) Å), which is as expected (pK_a: $quinH^+$, 4.85; $bzimH^+$, 5.40; pyH^+, 5.14). The two Cu–Cl distances in 6 are almost equal (2.360(8), 2.354(7) Å) while those in 4 are different (*cf.* above), which is in contrast to complex **4** in which the axial Cu–Cl1 bond is longer than the equatorial Cu–Cl2 bond. Also, the Cu–Cl bond distances are comparable to those found in the CuN_3Cl_2 complex[63,64] (2.302(1) Å) with almost a similar geometry.

Electronic and EPR spectra: solution structures of copper(II) complexes

All the complexes are soluble in water, stable in air and non-hygroscopic. The electronic absorption spectra of all the complexes are very similar to each other and show a low energy ligand field (LF) band (648–702 nm, Table 3) and a high energy ligand-based band (256–303 nm, Table 3). The intense band observed for **1** and **2** in the 355–370 nm range is assigned to the phenolate-to-Cu(II) LMCT transition (Table 3). The LF band energies (648, 655 nm) of complexes **1** and **2** are much higher than those of 3N ligand complexes (667–702 nm), which is expected of the stronger coordination of phenolate ligands. The LF energy of **2** (Fig. 5) is slightly

Table 3 Electronic absorption and EPR spectral properties of Cu(II) complexes

	λ_{max}, nm (ε, M^{-1} cm^{-1})[a]			EPR spectra[d]	
Complex	Ligand field[b]	Ligand based[c]	CT transition	Frozen solution[e]	
[Cu(L1)Cl] **1**	655 (58)	276 (13 750) 269 (16 083)	355 (2907)	$g_{\|\|}$ $g_\perp$ $A_{\|\|}$ $g_{\|\|}/A_{\|\|}$	2.272 2.073 166 137
[Cu(L2)Cl] **2**	648 (88)	276 (20 616) 270 (22 200)	367 (4288)	$g_{\|\|}$ $g_\perp$ $A_{\|\|}$ $g_{\|\|}/A_{\|\|}$	2.270 2.059 169 134
[$Cu(L3)Cl_2$] **3**	667 (54)	296 (5500) 288 (4450)	Shoulder	$g_{\|\|}$ $g_\perp$ $A_{\|\|}$ $g_{\|\|}/A_{\|\|}$	2.245 2.049 172 130
[$Cu(L4)Cl_2$] **4**	671 (70)	286 (12 033)	Shoulder	$g_{\|\|}$ $g_\perp$ $A_{\|\|}$ $g_{\|\|}/A_{\|\|}$	2.258 2.054 174 129
[$Cu(L5)Cl_2$] **5**	680 (45)	303 (8350) 276 (8033) 269 (7566)	—	$g_{\|\|}$ $g_\perp$ $A_{\|\|}$ $g_{\|\|}/A_{\|\|}$	2.274 2.073 155 147
[$Cu(L6)Cl_2$] **6**	702 (80)	256 (30 216) 336 (8650)	—	$g_{\|\|}$ $g_\perp$ $A_{\|\|}$ $g_{\|\|}/A_{\|\|}$	2.241 2.069 145 154

[a] In methanol. [b] Concentration, 5×10^{-3} M. [c] Concentration, 6×10^{-5} M. [d] In methanol–acetone (4 : 1) glass at 77 K. [e] Concentration, 5×10^{-3} M. $A_{||}$ is 10^{-4} cm^{-1}.

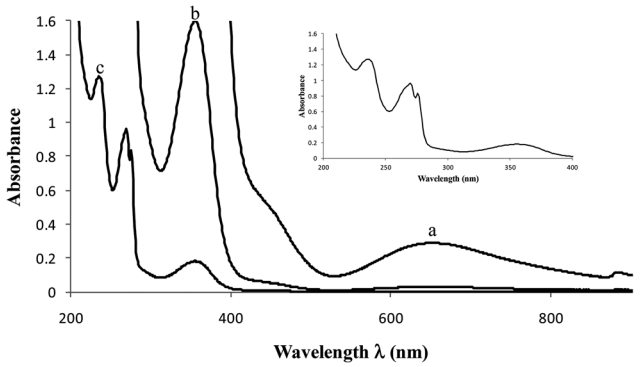

Fig. 5 Electronic absorption spectra of 5 mM complex [Cu(L1)Cl] **1** in water. [a]5.0 × 10^{-3} M, [b]5.5 × 10^{-4} M, [c]6.2 × 10^{-5} M. Inset graph: Expanded (200–400 nm) electronic spectra of **1** at 6.2 × 10^{-5} M concentration.

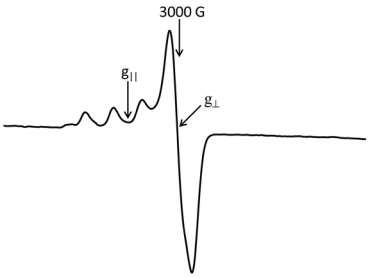

Fig. 6 X-band EPR spectra of complex **1** in frozen water–ethyleneglycol (4 : 1) glass at 77 K. (Frequency 9.09 GHz).

higher than **1** suggesting the stronger coordination of the phenolate moiety with electron-releasing methyl substituent, which is evident from the shorter Cu–$O_{phenolate}$ bond in the X-ray structure of **2**. The LF energy of the 3N ligand complexes varies in the order **3** (py,py) ≥ **4** (py,bzim) > **5** (im,bzim) > **6** (quin,bzim), which is consistent with the steric effect of the quinolyl moiety conferring enhanced distortion on the Cu(II) coordination geometry (*cf.* above) and the coordination of the imidazole nitrogen stronger than the pyridine nitrogen.

The frozen solution EPR spectra of all the complexes exhibit spectral features typical of mononuclear Cu(II) species. They are axial with $g_{||} > g_{\perp} > 2.0$ and $G = [(g_{||} - 2)/(g_{\perp} - 2)] = 3.7–4.6$, suggesting the presence of a $d_{x^2-y^2}$ ground state in copper(II) located in square-based geometries.[65,66] A square-based CuN_4 chromophore is expected[67–69] to show a $g_{||}$ value of 2.200 and an $A_{||}$ value in the range of 180–200 × 10^{-4} cm^{-1}, and the replacement of a coordinated nitrogen in this chromophore by oxygen is expected to enhance the $g_{||}$ value and decrease the $A_{||}$ value. Also, any distortion from planarity of square planar coordination geometry would also increase the $g_{||}$ and decrease the $A_{||}$ value. So the observed values of $g_{||}$ (2.241–2.274) and $A_{||}$ (145–174 × 10^{-4} cm^{-1}) for **3–4** are consistent with CuN_3O/CuN_3Cl chromophore of the complexes in solution. The low $A_{||}$ values suggest that there is significant distortion from planarity, which is evident from the X-ray crystal structures of **4** and **6** (Fig. 6, *cf.* below). The value of $g_{||}/A_{||}$ quotient for complexes **5** (149 cm) and **6** (154 cm) are higher than the range (105–135 cm) for complexes with a perfect square planar coordination geometry. This suggests that the coordination geometries in **5** and **6** are strongly distorted from planarity. In fact, the values of their $g_{||}/A_{||}$ quotient (**5**: 146, **6**: 155 cm) are higher than **4**, because of the incorporation of sterically demanding bzim (**5**) and/or quinolyl moiety (**6**) in the place of pyridyl moiety in **4**. Further, the $g_{||}$ values of **1** and **2** are higher and their $A_{||}$ value lower than those for **3–6** and the $g_{||}/A_{||}$ values fall within the range for square planar complexes with no or slight geometrical distortion and this is consistent with the above X-ray structures and electronic spectral results. The ESI-MS data reveal that the complexes retain their identity even in solution (Fig. 7). This is supported by the values of molar conductivity of the complexes in acetonitrile (Λ_M/Ω^{-1} 6–8 cm^2 mol^{-1}), which suggests that chloride ions remain coordinated to copper(II).

Electrochemical studies

The cyclic (CV) and differential pulse voltammetric (DPV) responses obtained in methanol solution reveal that the Cu(II)/Cu(I) redox couple of **3–6** are far from reversible (Table 4, $E_{1/2}$, −0.121 to −0.327 V; Fig. 8). The complexes **1–2**, which contain phenolate ligands, do not show any reproducible CV responses possibly due to phenoxide radical formation rendering the complex unstable. The E_{pc} values of the 3N ligand complexes follow the trend **3** (−0.407) < **4** (−0.381) < **5** (−0.350) < **6** (−0.219). It is well-known[70,71] that the incorporation of im moiety in the coordination sphere raises the Cu(II)/Cu(I) redox potential of the complexes by approximately 52 mV and that of bulky bzim moiety by approximately 165 mV, by destabilizing the Cu(II) oxidation state. Thus, upon replacement of the pyridyl moiety in **4** by imidazolyl moiety as in **5**, there is a positive shift (30 mV) in the $E_{1/2}$ value. However, upon replacing the pyridyl moiety in **3** by bzim moiety as in **4**, the redox potential becomes only slightly more positive (25 mV). On the other hand, on the replacement of the pyridyl moiety in **4** by quinolyl moiety as in **6**, the redox potential is shifted (160 mV) enormously to a more positive value, suggesting that the bulky quinolyl moiety distorts[70,71] the Cu(II) coordination geometry from planar geometry and renders the Cu(II) to Cu(I) electron-transfer more facile.

DNA binding studies

Absorption spectral studies. The B-form DNA is a polyanion composed of two complementary polymeric subunits hydrogen bonded together in the form of a right-handed double helix.[72] When the mono- and dicationic complexes of tridentate ligands interact with DNA, they are likely to replace two sodium cations from the compact inner (Stern) layer or the diffuse outer layer surrounding DNA and interact with the anionic phosphate residues of DNA.[73] The one/two labile chloride ion(s) of the complexes can be replaced by one or more nucleophiles in DNA, usually nitrogenous bases such as guanine (N7), leading to strong DNA binding of the complexes.[74] In some cases, binding to the adenine (N7) nitrogen

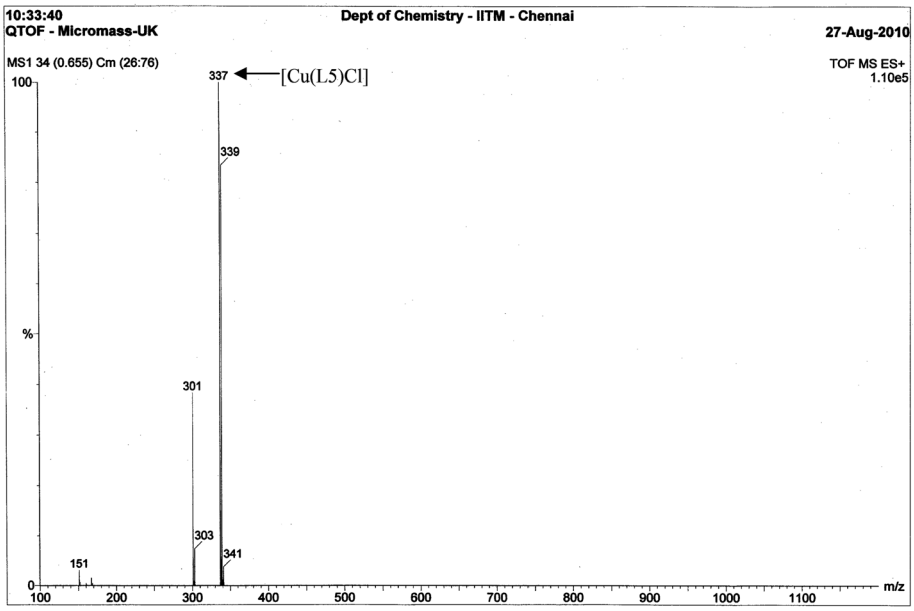

Fig. 7 ESI-MS spectra of $[Cu(L5)Cl]^+$ in methanol.

Table 4 Cyclic voltammetric behavior[a] of copper(II) complexes at 25.0 ± 0.2 °C in methanol

Complex	E_{pc}(CV) (V)	$E_{1/2}$(DPV) (V)	Redox process
$[Cu(L3)Cl_2]$ **3**	−0.407	−0.327	Cu(II) → Cu(I)
$[Cu(L4)Cl_2]$ **4**	−0.381	−0.311	Cu(II) → Cu(I)
$[Cu(L5)Cl_2]$ **5**	−0.350	−0.271	Cu(II) → Cu(I)
$[Cu(L6)Cl_2]$ **6**	−0.219	−0.121	Cu(II) → Cu(I)

[a] Measured *vs.* Ag/Ag^+ electrode; scan rate, 50 mV s^{-1}; supporting electrolyte TBAP (100 mM); complex concentration 1 mM.

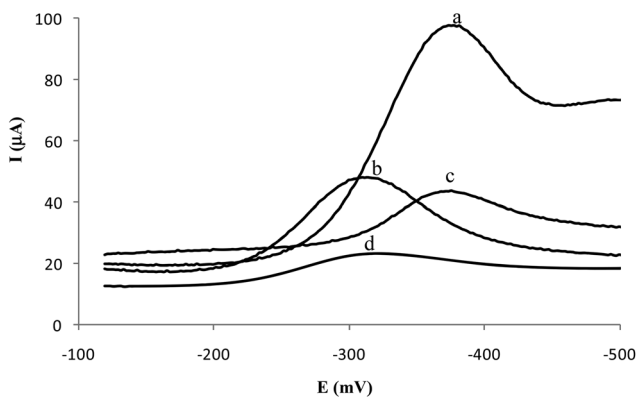

Fig. 8 Differential pulse voltammograms of 0.001 M complexes a, b, c, d; **3**, **4**, **5** and **6** in methanol solution at 25 °C at 5 mV s^{-1} scan rate.

has been also observed but to a lesser extent. Other coordination sites present on the nucleic acid such as N1 atom of purine and N3 atom of pyrimidine in the double-stranded helix are not easily accessible. Hence, extensive studies on the interaction of different tridentate ligand complexes with DNA are needed to evaluate the factors affecting the DNA binding mode. The Cu(II) complexes of the 2NO (**1**, **2**) and 3N (**3**–**6**) ligand systems with aromatic py/bzim moiety and labile chloride ions have the potential to bind to DNA covalently to form CuN_3O and CuN_4 chromophores respectively. A similar covalent mode of DNA binding has been established[23] for complexes of the type $[Cu(L)Cl_2]$, where L is a linear tridentate 3N ligand by using UV-Vis and EPR spectroscopy.

Upon the incremental addition of CT DNA to **1**–**2**, the ligand centered π→π* absorption bands (**1**, 235; **2**, 242; **1**, **2**: 276 nm) show a decrease in molar absorptivity (hypochromism: **1** ~12; **2** ~8%) with no red-shift (Table 5, Fig. 9) at R = 25 (R = [DNA]/[Cu]; [Cu] = 2.0×10^{-5} M). It is possible that

Table 5 Ligand based absorption spectral properties of Cu(II) complexes on binding to CT DNA[a]

Complex	λ_{max} (nm)	R	$\Delta\varepsilon^e$ (%)	R	$\Delta\varepsilon^e$ (%)	$K_b \times 10^3$ M^{-1}
$[Cu(L1)Cl]$ **1**	235[b]	10	7.5	25	11.6	10.0
	276[b]	10	8.6	25	11.5	16.0
	276[c]	10	68.0	25	94.0	—
$[Cu(L2)Cl]$ **2**	242[b]	10	3.8	25	8.0	8.0
	276[b]	10	3.0	25	7.7	8.2
	276[c]	10	28.0	25	90.0	—
$[Cu(L3)Cl_2]$ **3**	287[c]	10	31.0	25	47.0	[d]
$[Cu(L4)Cl_2]$ **4**	287[c]	10	74.0	25	88.0	[d]
$[Cu(L5)Cl_2]$ **5**	276[c]	10	32.0	25	53.0	3.0
$[Cu(L6)Cl_2]$ **6**	336[c]	10	53.0	25	57.0	6.6

[a] R = [DNA]/[Cu]. [b] Concentration of copper complexes = 2.0×10^{-5} M. [c] Concentration of copper complexes = 6.0×10^{-5} M. [d] K_b could not be calculated as saturation behavior is not observed in the absorption spectral titration. [e] Hypochromism.

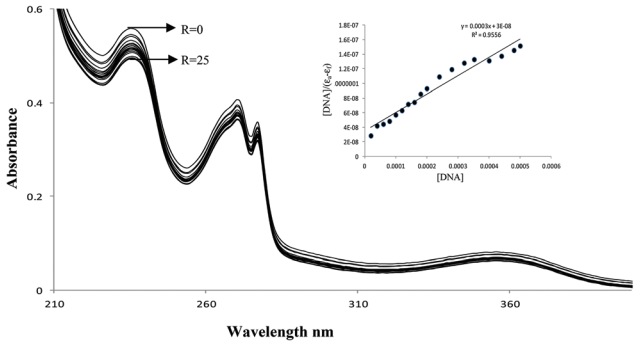

Fig. 9 Absorption spectra of [Cu(L1)Cl] **1** (2×10^{-5} M) in 5 mM Tris HCl buffer at pH 7.2 in the absence (R = 0) and presence of (R = 25) increasing amounts of DNA.

at higher concentrations of DNA more DNA binding sites are available and the copper complexes tend to bind completely to DNA. Interestingly, at higher concentrations of complexes the 276 nm band shows a strong hypochromism (**1**, 68; **2**, 28%) at R = 10, and stronger hypochromism (**1**, 94; **2**, 90%) at R = 25. It is possible that monomeric phenolate complexes would dimerise[63] in the presence of higher concentrations of chloride ions, and interact more strongly with CT DNA causing stronger hypochromism and disappearance of the ligand based band. From the changes in the spectra at the lower concentration, the DNA binding constant (K_b) has been calculated, by using the equation

$$[\mathrm{DNA}]/(\varepsilon_a - \varepsilon_f) = [\mathrm{DNA}]/(\varepsilon_b - \varepsilon_f) + 1/K_b(\varepsilon_b - \varepsilon_f).$$

The K_b values of **1** (10.0×10^3 M^{-1}) and **2** (8.0×10^3 M^{-1}) are almost the same, which is expected of their very similar molecular structures. Among the 3N ligand complexes **3–6**, the observed trend in hypochromism is **3** (47%) < **4** (88%) > **5** (53%) ≥ **6** (57%) at R = [DNA]/[Complex] = 25. Upon replacing the pyridyl moiety in [Cu(L3)Cl_2] **3** by bzim moiety to give [Cu(L4)Cl_2] **4** the DNA binding affinity increases enormously. The hydrogen bonding interactions of bzim-NH with the nucleobases present on the edge of the DNA[75] as well as the hydrophobic interaction of bzim moieties with DNA surface are expected to contribute significantly to the higher DNA binding affinities of the bzim-based complexes.[31] This is supported by the observation that on the incorporation of σ-bonding imidazole moiety in the place of pyridyl moiety in **4** to give **5**, the DNA binding affinity decreases. However, the quinolyl moiety present in **6** is involved in strong hydrophobic DNA interaction like the bzim moiety and so exhibit DNA binding affinity higher than **5**. For **5** and **6** the values of the DNA binding constant (K_b) calculated by using the above equation are 3.0×10^3 M^{-1} and 6.6×10^3 M^{-1} respectively. The K_b values for **3** and **4** could not be calculated as they do not exhibit saturation behavior in DNA binding. The order of DNA binding constants (K_b) of the complexes is **1** (10.0) > **2** (8.0) < **5** (3.0) < **6** (6.6×10^3 M^{-1}). The 3N ligand complexes **3–6** possess DNA binding affinity lower than the phenolate ligand complexes (**1–2**), which is expected of the dicationic nature of the former complexes. Thus all the above observations indicate that the complexes containing easily displaceable chloride ions bind *via* covalent interaction with DNA like cisplatin (*cis*-[$Pt(NH_3)_2Cl_2$]) to form novel DNA adduct species and the bzim ligand moiety and dicationic nature of the complexes appear to facilitate the DNA binding.

Competitive DNA-binding studies. A competitive ethidium bromide (EthBr) DNA binding study was undertaken to understand the mode of DNA interaction of the copper(II) complexes. The molecular fluorophore EthBr emits intense fluorescence in the presence of CT DNA due to its strong intercalation in between the adjacent DNA base pairs. Addition of a second molecule, which binds to DNA more strongly than EthBr, would displace bound EthBr and quench the DNA-induced EthBr emission.[28] The extent of quenching of the fluorescence of EthBr bound to DNA would reflect the extent of DNA binding of the second molecule. Upon adding **1–6** (0–60 μM) to CT DNA (125 μM) pretreated with EthBr (12.5 μM) ([DNA]/[EthBr] = 25) in 5% DMF–5 mM Tris-HCl–50 mM NaCl buffer at pH 7.1, the emission intensity of DNA-bound EthBr decreases enormously (Fig. 10). All the complexes quench the emission intensity of ethidium bromide completely at higher R values. Addition of a second DNA-binding molecule would quench the EthBr emission by either replacing the DNA-bound EthBr (if it binds to DNA more strongly than EthBr) and/or by

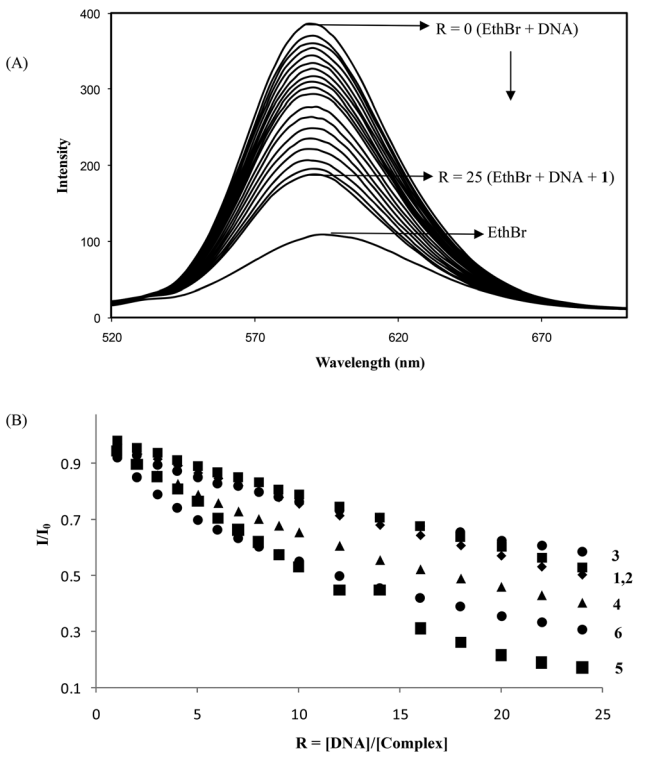

Fig. 10 (A) Effect of addition of complex **1** on the emission intensity of the CT DNA-bound ethidium bromide in 5 mM Tris-HCl–50 mM NaCl buffer at pH 7.1. (B) Effect of addition of all the complexes on the emission intensity of the CT DNA-bound ethidium bromide in 5 mM Tris-HCl–50 mM NaCl buffer at pH 7.1.

accepting the excited state electron from EthBr. The observed abilities of both the copper(II)-phenolate complexes to quench the DNA induced EthBr emission is almost the same and are higher than those for the 3N ligand complexes, which is consistent with the absorption spectral results (*cf.* above). As it is very difficult for the present complexes with no extended planar rings to displace the intercalatively bound EthBr, the EthBr displacement mechanism may be ruled out. If the quenching occurs by photo electron-transfer mechanism, then the ability of the complexes to quench the EthBr emission intensity would depend upon the reducibility of the copper(II) complexes (*cf.* above) and so parallel the variation in the $E_{1/2}$ values of the Cu(II)/Cu(I) redox potential: **3** (−0.407 V) < **4** (−0.381 V) < **5** (−0.350 V) < **6** (−0.219 V). The apparent DNA binding constant (K_{app}) was calculated from a plot of the observed intensities against the complex concentration used to titrate with DNA pretreated with EthBr using the equation

$$K_{EthBr}\ [EthBr] = K_{app}\ [complex]$$

where K_{EthBr}, which equals $1.0 \times 10^7\ M^{-1}$,[76] is the DNA binding constant of EthBr, [EthBr] is the concentration of EthBr (12.5 μM) and [complex] is the concentration of the complex used to obtain 50% reduction in fluorescence intensity of DNA pretreated with EthBr. As expected, the observed ability of the 3N ligand complexes to quench the DNA induced EthBr emission and DNA binding constant (K_{app}) decreases in the order, **3** ($3.4 \times 10^4\ M^{-1}$) < **4** ($4.3 \times 10^4\ M^{-1}$) < **5** ($7.2 \times 10^4\ M^{-1}$) < **6** ($7.6 \times 10^4\ M^{-1}$). The complex **6** with a more positive redox potential has the highest ability to quench the emission intensity of EthBr. The order of K_{app} values **3** < **4** < **5** < **6** are consistent with the trend in hypochromism determined from absorption spectral studies.

Chemical nuclease activity of complexes and mechanistic investigations

Oxidative cleavage of DNA. The ability of the present complexes to effect oxidative DNA cleavage has been investigated by gel electrophoresis using supercoiled pUC19 DNA (40 μM) in 5 mM Tris-HCl–50 mM NaCl buffer (pH 7.1) in the presence of H_2O_2 (100 μM). The control experiments with H_2O_2 alone or $CuCl_2$ and H_2O_2 do not show any DNA cleavage activity. However, our present complexes effect more efficient DNA cleavage activity oxidatively in the presence of H_2O_2. At 50 μM concentration all the complexes convert SC DNA (Form I) into nicked circular (NC) DNA (form II) with prominent DNA cleavage (**1**, 50; **2**, 40; **3**, 50; **4**, 45; **5**, 95; **6**, 100%, Fig. 11 and 12, Table 6). It is remarkable that **5** and **6** completely degrade SC DNA into undetectable minor fragments. For these complexes concentration dependent DNA cleavage experiments were carried out, keeping the concentration of DNA (40 μM in base pairs) constant. It is clearly seen that even at 40 μM concentration **5** effects efficient DNA cleavage (NC DNA, 90%) (Fig. 13 and 14). As the concentrations of **5** and **6** are increased, the amount of NC DNA (form II) increases and reaches a maximum (complete conversion) at nearly 50 μM

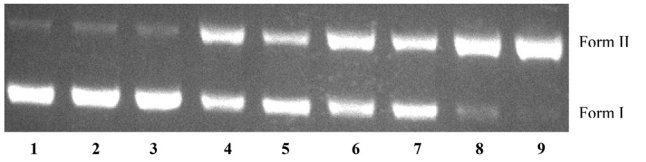

Fig. 11 Gel electrophoresis diagram showing the oxidative cleavage of supercoiled pUC19 DNA (40 μM in base pair) by complexes **1–6** (50 μM) in 5 mM Tris-HCl–50 mM NaCl buffer at pH 7.1 and 37 °C with an incubation time of 1 h in the presence of hydrogen peroxide (100 μM). Lane 1, DNA; lane 2, DNA + H_2O_2; lane 3, DNA + $CuCl_2$ + H_2O_2; lane 4, DNA + **1** + H_2O_2; lane 5, DNA + **2** + H_2O_2; lane 6, DNA + **4** + H_2O_2; lane 7, DNA + **5** + H_2O_2; lane 8, DNA + **6** + H_2O_2; lane 9, DNA + **3** + H_2O_2.

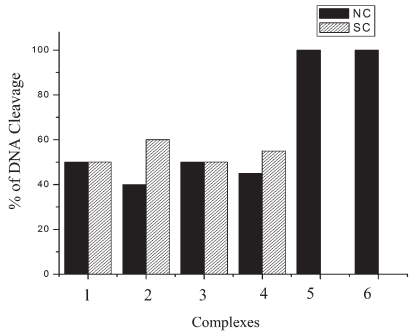

Fig. 12 Percentage of oxidative DNA cleavage efficiencies of complexes **1–6** (50 μM) showing an increase in form II (NC DNA) with 1 h an incubation time of 1 h.

Table 6 Cleavage data of SC pUC19 DNA (40 μM in base pair) by complexes **1–6** (50 μM) in the presence of H_2O_2 for an incubation time of 1 h

		Form %	
Serial no.	Reaction condition	SC	NC
1	DNA control	95	5
2	DNA + H_2O_2	95	5
3	DNA + $CuCl_2$ + H_2O_2	95	5
4	DNA + H_2O_2 + **1**	50	50
5	DNA + H_2O_2 + **2**	60	40
6	DNA + H_2O_2 + **3**	50	50
7	DNA + H_2O_2 + **4**	55	45
8	DNA + H_2O_2 + **5**	5	95
9	DNA + H_2O_2 + **6**	0	100

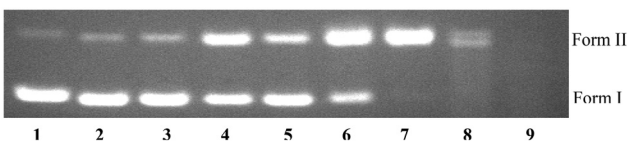

Fig. 13 Gel electrophoresis diagram showing the oxidative cleavage of supercoiled pUC19 DNA (40 μM in base pair) by complex **5** at different concentrations in 5 mM Tris-HCl–50 mM NaCl buffer at pH 7.1 and 37 °C with an incubation time of 1 h in the presence of hydrogen peroxide (100 μM). Lane 1, DNA; lane 2, DNA + H_2O_2; lane 3, DNA + **5** (10 μM) + H_2O_2; lane 4, DNA + **5** (20 μM) + H_2O_2; lane 5, DNA + **5** (30 μM) + H_2O_2; lane 6, DNA + **5** (40 μM) + H_2O_2; lane 7, DNA + **5** (50 μM) + H_2O_2; lane 8, DNA + **5** (80 μM) + H_2O_2; lane 9, DNA + **5** (100 μM) + H_2O_2.

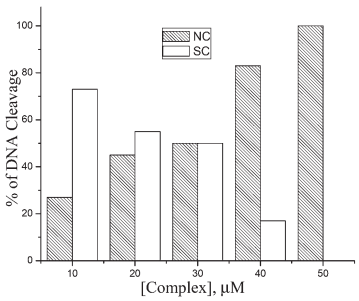

Fig. 14 Percentage of oxidative DNA cleavage efficiencies of complex **5** (10 to 50 μM) showing an increase in form II (NC DNA) with an incubation time of 1 h.

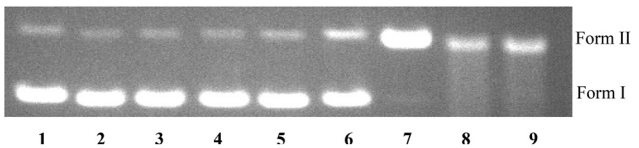

Fig. 15 Gel electrophoresis diagram showing the oxidative cleavage of supercoiled pUC19 DNA (40 μM in base pair) by complex **6** at different concentrations in 5 mM Tris-HCl–50 mM NaCl buffer at pH 7.1 and 37 °C with an incubation time of 1 h in the presence of hydrogen peroxide (100 μM). Lane 1, DNA; lane 2, DNA + H_2O_2; lane 3, DNA + **6** (10 μM) + H_2O_2; lane 4, DNA + **6** (20 μM) + H_2O_2; lane 5, DNA + **6** (30 μM) + H_2O_2; lane 6, DNA + **6** (40 μM) + H_2O_2; lane 7, DNA + **6** (50 μM) + H_2O_2; lane 8, DNA + **6** (80 μM) + H_2O_2; lane 9, DNA + **6** (100 μM) + H_2O_2.

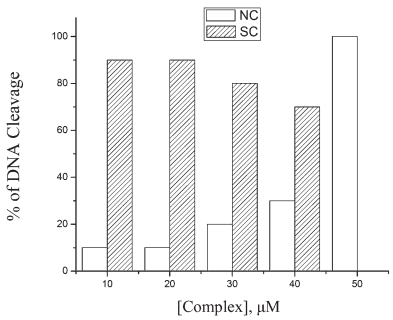

Fig. 16 Percentage of oxidative DNA cleavage efficiencies of complex **6** (10 to 50 μM) showing an increase in form II (NC DNA) with an incubation time of 1 h.

concentration, and smearing occurs at higher concentrations (Fig. 15 and 16). As the linear form of DNA (form III) is not at all observed under the present conditions, it is clear that DNA cleavage occurs randomly because a significant portion of plasmid DNA is already converted to the NC form without the concurrent formation of the linear form. The intense nuclease activities of **5** and **6** are apparently due to enhanced stabilization of their Cu(I) species (*cf.* below) through increased π-delocalization involving the imidazolyl/quinolyl moiety (*cf.* above), which is evident from their more positive Cu(II)/Cu(I) redox potential. As the concentration of hydrogen peroxide is increased from 10 to 100 μM, keeping those of **6** (50 μM) and DNA constant, the amount of form I decreases while that of form II increases (Fig. 17). Interestingly, **6** causes cleavage of

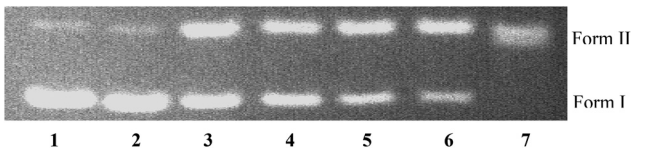

Fig. 17 Gel electrophoresis diagram showing the oxidative cleavage of supercoiled pUC19 DNA (40 μM in base pair) by complex **6** (50 μM) in 5 mM Tris-HCl–50 mM NaCl buffer at pH 7.1 and 37 °C with an incubation time of 1 h in the presence of varying concentrations of hydrogen peroxide. Lane 1, DNA; lane 2, DNA + H_2O_2 (100 μM); lane 3, DNA + **6** + H_2O_2 (20 μM); lane 4, DNA + **6** + H_2O_2 (40 μM); lane 5, DNA + **6** + H_2O_2 (60 μM); lane 6, DNA + **6** + H_2O_2 (80 μM); lane 7, DNA + **6** + H_2O_2 (100 μM).

more than 50% of DNA even at 20 μM hydrogen peroxide concentration. In contrast, **3** and **4** show moderate cleavage activity, which is consistent with their less positive Cu(II)/Cu(I) redox potential (*cf.* above). The complexes **1** and **2** also show moderate DNA cleavage activity at 50 μM concentration in the presence of 100 μM hydrogen peroxide for an incubation time of 1 h.

The preliminary mechanism of oxidative cleavage of pUC19 plasmid DNA by **1–6** was studied by adding various radical inhibitors to the reaction mixtures. When the hydroxyl radical scavenger DMSO is added, around 20% of inhibition of DNA cleavage is observed, revealing that the cleavage reaction involves $^{\cdot}OH$ radicals (Fig. 18 and 19). The addition of NaN_3

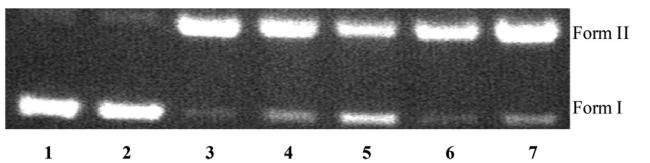

Fig. 18 Gel electrophoresis diagram showing the oxidative cleavage of supercoiled pUC19 DNA (40 μM in base pair) by complex **6** (50 μM) in the presence of various radical scavengers in a 5 mM Tris-HCl–50 mM NaCl buffer at pH 7.1 and 37 °C with an incubation time of 1 h in the presence of hydrogen peroxide (100 μM). Lane 1, DNA; lane 2, DNA + H_2O_2; lane 3, DNA + **6** + H_2O_2; lane 4, DNA + **6** + H_2O_2 + ethanol; lane 5, DNA + **6** + H_2O_2 + 10% DMSO; lane 6, DNA + **6** + H_2O_2 + NaN_3 (100 μM); lane 7, DNA + **6** + H_2O_2 + SOD (1 unit).

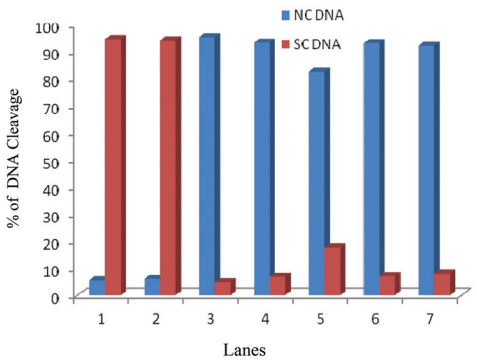

Fig. 19 Percentage of oxidative DNA cleavage efficiencies of complex **6** in the presence of different types of radical quenchers.

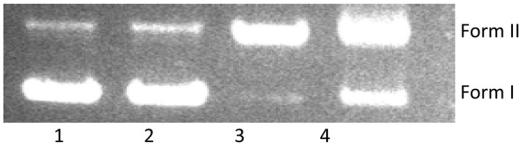

Fig. 20 Gel electrophoresis diagram showing the oxidative cleavage of supercoiled pUC19 DNA (40 μM in base pair) by complex **6** (50 μM) in the presence of catalase in a 5 mM Tris-HCl–50 mM NaCl buffer at pH 7.1 and 37 °C with an incubation time of 1 h in the presence of hydrogen peroxide (100 μM). Lane 1, DNA; lane 2, DNA + H_2O_2; lane 3, DNA + **6** + H_2O_2; lane 4, DNA + **6** + H_2O_2 + catalase (10 units).

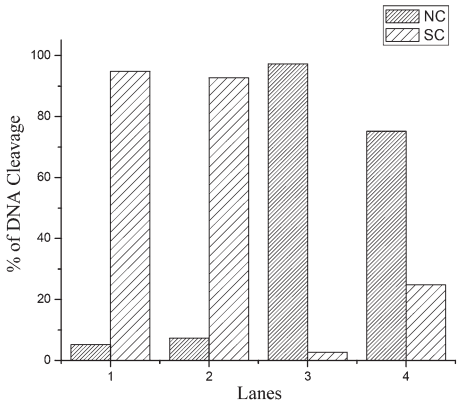

Fig. 21 Percentage of oxidative DNA cleavage efficiencies of complex **6** in the presence of catalase enzyme.

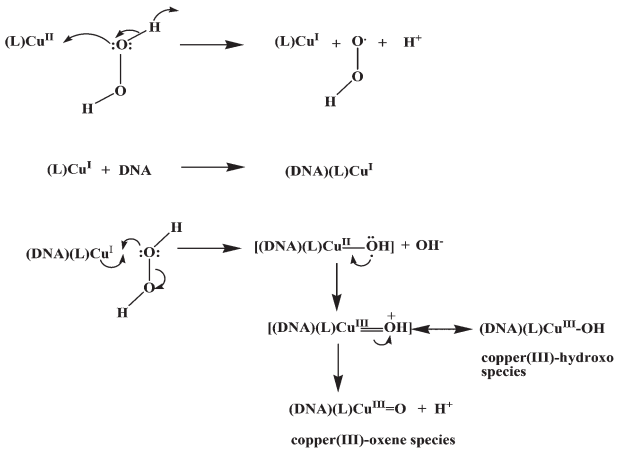

Scheme 2 Mechanism of DNA cleavage.

also does not prevent the cleavage of DNA by **6**, suggesting that neither $^1O_2$ nor any other singlet oxygen-like entity participates in the oxidative DNA cleavage. Also, as the addition of catalase enzyme inhibits only slightly (up to 25%) the breakdown of the DNA, the participation of hydrogen peroxide in the cleavage process could not be ruled out (Fig. 20 and 21). Further, addition of superoxide dismutase (superoxide scavenger) does not quench the cleavage reaction significantly, revealing that superoxide anion is also not the active species.[77] The results show that none of the reactive species, namely, $^1O_2$ or O_2^- but $^{\cdot}OH$ radicals are involved in the DNA cleavage reaction, and that a copper–oxygen species might be responsible for DNA cleavage. We propose that, in the first step, the complex (L)Cu(II) is reduced by H_2O_2 to form the (L)Cu(I) species, which binds to DNA forming the (DNA)(L)Cu(I) adduct (eqn (1) and (2), Scheme 2).[25,78–83] The adduct then reacts with another equivalent of H_2O_2 to generate free hydroxide ion and DNA bound Cu(II)-hydroxyl radical intermediate by the Haber–Weiss mechanism (eqn (3)).[83] The latter forms a 'DNA bound copper-oxene' or a resonance hybrid of a DNA bound copper(II)-hydroxyl radical and a putative copper(III)-oxene/Cu(III)-hydroxo species, which generates a deoxyribose-centered radical by C-1/C-4 hydrogen abstraction (Scheme 3).[30,79,84] In order to throw light on the mechanism and the active species involved in the oxidative DNA cleavage, the reaction of the copper(II) complexes with H_2O_2 was studied. Addition of H_2O_2 (5% equiv.) to 1 mM acetonitrile solution of **1–6** causes a rapid decoloration from blue-green to yellow, indicating the formation of Cu(III) species like metal-oxo and metal-hydroxo species, which are expected to cleave the DNA backbone, but are not expected to be quenched by hydroxyl radical quenchers.[85,86] Reglier *et al.* have used a similar kind of decoloration experiment to show the involvement of copper(III) species in the DNA cleavage mechanism.[79] Sigman *et al.* have also proposed the same kind of Cu(III)-oxene species, which is responsible for the DNA cleavage mechanism for the $[Cu(phen)_2]^{2+}$ complex.[87] Very recently, we have reported that a putative copper(III)-oxene/Cu(III)-hydroxo species, which generates a deoxyribose-centered radical by C-1 hydrogen abstraction, is the one responsible for DNA cleavage.[32] It may be noted that complexes capable of covalent interaction with DNA generate Cu(III)-oxene species as the reactive intermediate in the DNA cleavage process but their DNA cleavage ability is not significant in comparison with complexes involved in non-covalent DNA interaction. The latter brings about more effective DNA cleavage by locating themselves near the site of DNA cleavage through non-covalent interaction of diimine co-ligands and generating more reactive hydroxyl radicals.[31,35–37] Thus, the simple Cu(II)–phenolate complexes without diimine co-ligands as DNA recognition elements are not efficient DNA-cleaving agents because the vacant axial site is not readily available for the formation of Cu(III)-hydroxide radical species due to the strong coordination of the phenolate moiety to the Cu(II) center.[35,37] However, the present simple 3N ligand complexes without diimine co-ligands provide a vacant axial site very readily available for attack by H_2O_2 to form hydroxyl radicals. Thus the complexes capable of covalent interaction with DNA are less efficient DNA cleaving agents than the non-covalently DNA binding mixed-ligand complexes.

In the second step of the mechanism a CH-1′ and/or CH-4′-atom abstraction by the copper(III) species takes place leading to the radical precursor of DNA degradation products (Scheme 3).

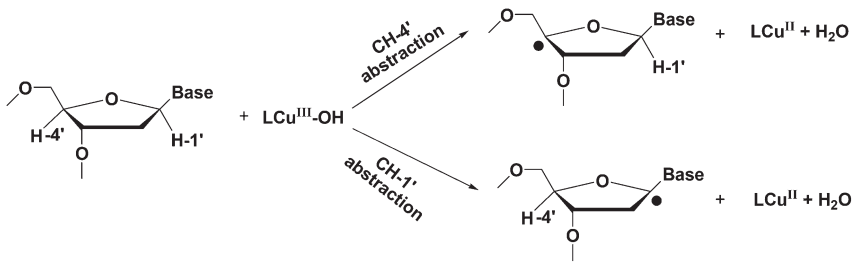

Scheme 3 Mechanism of DNA cleavage (CH-1′ and CH-4′ abstraction) (ref. 79).

Anticancer activity studies

MTT assay. As several redox-active metal complexes showing DNA cleavage exhibit anticancer activity,[31,35–37] the cytotoxicity of the present copper(II) complexes, which have the ability to strongly bind and oxidatively cleave DNA, was investigated against the HBL-100 human breast cancer cell line in aqueous buffer solution in comparison with the widely used drug cisplatin under identical conditions by using an MTT assay. All the complexes show prominent cytotoxicity and the IC_{50} values obtained (Table 6) by plotting the cell viability against concentration of the complexes reveal that all of them exhibit cytotoxicity higher than cisplatin for 24 h incubations (IC_{50}, 25 μM). Also, the IC_{50} values at 48 h are lower than those at 24 h clearly indicating that the cell killing ability is dose and time dependent. Further, as revealed by the observed IC_{50} values (8.6–21.4 μM, Table 7), the potency of the copper–phenolate complexes to kill the cancer cells follows the order **1** >**2**, while that of the 3N complexes follows the order **3** >**4** <**5** ≈ **6**. We have already shown that covalently DNA binding simple Cu(II) complexes exhibit lower cell killing activity than their mixed ligand Cu(II) complexes of diimine co-ligands.[31,35–37] So it is clear that the non-covalently DNA binding complexes are excellent cytotoxic agents than the covalently DNA binding complexes. We have already established that copper(II) complexes, which exhibit higher DNA binding affinity and prominent DNA cleavage activity, display efficient cytotoxicity and anticancer properties.[31,35–37] Thus, interestingly, the phenolate ligand complexes show lower cell killing activity than the 3N ligand complexes, which moderately cleave DNA. However, the complex **3** with a lower DNA binding affinity and poor DNA cleavage activity shows anticancer activity more prominent than all the other 3N ligand complexes. This reveals that **3** exerts higher cytotoxicity through a mechanism which may not involve direct DNA binding and DNA cleavage, and that neither DNA binding nor DNA cleavage mechanism alone is an essential criterion for the present compounds to act as anticancer agents. In this regard it may be noted that the complexes $[Cu(tdp)(tmp)]^{+}$ [37] and $[Cu(pmdt)(dmp)]^{2+}$ [36] with enhanced hydrophobicity show poor DNA binding ability but strong protein binding affinity and exhibit higher cell killing activity. So, studies on the ability of complexes to bind with proteins may offer more insights into the factors that influence the anticancer activity of the copper(II) complexes. Also, more detailed and advanced studies are needed to fully understand the detailed molecular mechanism of cytotoxicity.

Lymphocyte cytotoxicity assay. The cytotoxic activity of complexes **1–6** against lymphocytes, which are normal white blood cells isolated from human blood samples, has been investigated. Interestingly, all the live normal cells appear as green colored fluorescence (Fig. 22) upon treatment with the complexes **1–6**, which reveals that the complexes are non-toxic to normal cells (lymphocytes).

Table 7 *In vitro* cytotoxicity assays for complexes **1–6**, cisplatin against the human breast cancer cell line (HBL-100) (data are mean ± SD of four replicates each)

	IC_{50}/μM by MTT assay[a]	
Complexes	24 h	48 h
[Cu(L1)Cl] **1**	18.5 ± 1.8	12.4 ± 1.3
[Cu(L2)Cl] **2**	21.4 ± 2.4	16.4 ± 1.7
$[Cu(L3)Cl_2]$**3**	8.6 ± 0.8	5.9 ± 0.5
$[Cu(L4)Cl_2]$**4**	17.6 ± 1.2	12.4 ± 1.0
$[Cu(L5)Cl_2]$**5**	12.4 ± 1.4	8.3 ± 0.9
$[Cu(L6)Cl_2]$**6**	12.9 ± 1.1	7.8 ± 0.9
Cisplatin	25.0	—

[a] IC_{50} = is the concentration of drug required to inhibit the growth of 50% of the cancer cells (μM).

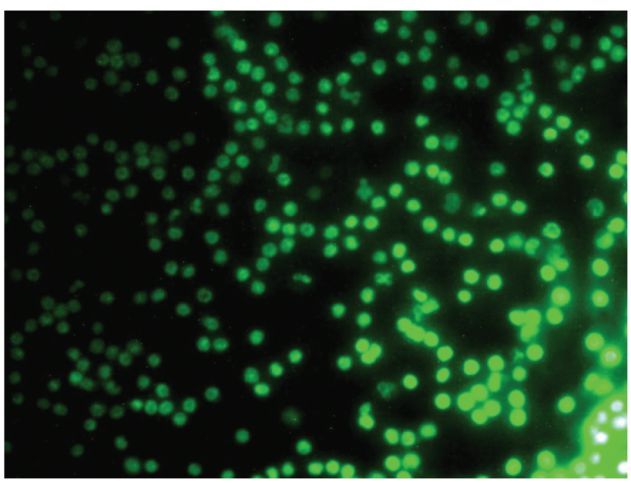

Fig. 22 Phase contrast microscope image of live lymphocytes stained with acridine orange (AO) upon treatment with complex **3**.

Conclusions

A series of water soluble copper(II) complexes of the types [Cu(L)Cl] and [Cu(L)Cl_2] have been isolated and their DNA binding affinities and DNA cleavage abilities studied. The phenolate ligand complexes [Cu(L)Cl] possess a distorted square-based geometry while the tridentate 3N ligand complexes [Cu(L)Cl_2] with pyridyl and quinolyl nitrogen donors possess a distorted trigonal bipyramidal geometry. All the complexes retain their identity even in solution, as diagnosed by absorption, EPR and ESI-MS spectral studies, and bind to DNA strongly. Both the absorption spectral titration and the EthBr displacement assay show that the complexes exhibit covalent mode of DNA interaction involving replacement of labile chloride ion. Also, all the complexes show significant DNA cleavage activity in the presence of hydrogen peroxide. Interestingly, the 3N ligand complexes with coordinated imidazolyl and quinolyl moieties show more positive Cu(II)/Cu(I) redox potential and exhibit chemical nuclease activity more prominent than the other complexes. It is proposed that they can act as artificial restriction enzymes in nucleic acid chemistry. All the complexes are remarkable in that they display cytotoxicity against the HBL-100 human breast cancer cell line more potent than the widely used drug cisplatin but are non-toxic to normal cells (lymphocytes); hence they can act as promising anticancer drugs. Further mechanistic and cellular uptake studies are essential to probe the higher potency of the complexes to kill cancer cells.

Acknowledgements

Professor M. Palaniandavar is a recipient of a Ramanna National Fellowship (Grant No. SR/S1/RFIC/01/2007-2010 & SR/S1/RFIC/01/ 2010-2013) of the Department of Science and Technology, New Delhi. We thank Indo French Centre for Promotion of Advanced Research (IFCPAR) for a collaborative project [Scheme No. IFC/A/4109-1/2009/993], DST Nano Mission Project (SR/NM/NS-110/2010 (G)) and a CSIR project (CSIR/01(2462)/11/EMR-II). UGC Grant No. F.4-1/2006(BSR)/7-22/2007 (BSR) is acknowledged for a JRF and SRF Fellowship to C.R. The X-ray diffraction, EPR and fluorescence spectral facilities in the Department were created by funding respectively from the Department of Science and Technology (DST-FIST), New Delhi and the University Grants Commission (SAP), New Delhi. We thank Dr K. Balakrishnan, Department of Immunology, School of Biological Sciences, Madurai Kamaraj University, Madurai for helping in micro lymphocytotoxicity assay study.

References

1 L. Ronconi and P. J. Sadler, *Coord. Chem. Rev.*, 2007, **251**, 1633–1648.
2 D. Wang and S. J. Lippard, *Nat. Rev. Drug Discovery*, 2005, **4**, 307–320.
3 P. C. A. Bruijnincx and P. J. Sadler, *Curr. Opin. Chem. Biol.*, 2008, **12**, 197–206.
4 J. A. Cowan, *Curr. Opin. Chem. Biol.*, 2001, **5**, 634–642.
5 J. K. Barton, *Science*, 1986, **233**, 727–734.
6 S. Dhar and A. R. Chakravarty, *Inorg. Chem.*, 2003, **42**, 2483–2485.
7 P. B. Dervan, *Science*, 1986, **232**, 464–471.
8 C. Hemmert, M. P. M. Renz, H. Gornitzka and S. S. B. Meunier, *J. Biol. Inorg. Chem.*, 2001, **6**, 14–22.
9 M. Navarro, E. J. Cisneros-Fajardo, A. Sierralta, M. Fernandez-Mestre, P. S. D. Arrieche and E. Marchan, *J. Biol. Inorg. Chem.*, 2003, **8**, 401–408.
10 E. Lamour, S. Routier, J. L. Bernier, J. P. Catteau, C. Bailly and H. J. Vezin, *J. Am. Ceram. Soc.*, 1999, **121**, 1862–1869.
11 R. Nagane, M. Chikira, H. Shindo and W. E. Antholine, *J. Inorg. Biochem.*, 2000, **78**, 243–249.
12 J. Liu, W. J. Mei, L. J. Lin, K. C. Zheng, H. Chao, F. C. Yun and L. N. Ji, *Inorg. Chim. Acta*, 2004, **357**, 285–293.
13 H. Chao, W. J. Mei, Q. W. Huang and L. N. Ji, *J. Inorg. Biochem.*, 2002, **92**, 165–170.
14 J. Z. Wu and L. Yuan, *J. Inorg. Biochem.*, 2004, **98**, 41–45.
15 D. S. Sigman, *Acc. Chem. Res.*, 1986, **19**, 180–186.
16 D. S. Sigman, A. Mazumder and D. M. Perrin, *Chem. Rev.*, 1993, **93**, 2295–2316.
17 S. Dhar, D. Senapati, P. K. Das, P. Chattopadhyay, M. Nethaji and A. R. Chakravarty, *J. Am. Chem. Soc.*, 2003, **125**, 12118–12124.
18 S. Y. Tsang, S. C. Tam, I. Bremner and M. J. Burkitt, *Biochem. J.*, 1996, **317**, 13–16.
19 A. Bencini, E. Berni, A. Bianchi, C. Giorgi, B. Valtancoli, D. K. Chand and H. J. Schneider, *Dalton Trans.*, 2003, **5**, 793–800.
20 D. K. Chand, H. J. Schneider, A. Bencini, A. Bianchi, C. Giorgi, S. Ciattini and B. Valtancoli, *Chem.–Eur. J.*, 2000, **6**, 4001–4008.
21 E. L. Hegg and J. N. Burstyn, *Coord. Chem. Rev.*, 1998, **173**, 133–165.
22 J. K. Barton and E. Lolis, *J. Am. Chem. Soc.*, 1985, **107**, 708–709.
23 A. Raja, V. Rajendiran, P. Uma Maheswari, R. Balamurugan, C. A. kilner, M. A. Halcrow and M. Palaniandavar, *J. Inorg. Biochem.*, 2005, **99**, 1717–1732.
24 S. Mahadevan and M. Palaniandavar, *Inorg. Chem.*, 1998, **37**, 693–700.
25 S. Mahadevan and M. Palaniandavar, *Inorg. Chem.*, 1998, **37**, 3927–3934.
26 S. Mahadevan and M. Palaniandavar, *Inorg. Chim. Acta*, 1997, **254**, 291–302.
27 M. Chikira, Y. Tomizava, D. Fukita, T. Sugizaki, N. Sugawara, T. Yamazaki, A. Sasano, S. Shindo, M. Palaniandavar and W. E. Anthroline, *J. Inorg. Biochem.*, 2002, **89**, 163–173.
28 P. Uma Maheswari and M. Palaniandavar, *J. Inorg. Biochem.*, 2004, **98**, 219–230.
29 P. Uma Maheswari and M. Palaniandavar, *Inorg. Chim. Acta*, 2004, **357**, 901–912.

30 P. Tamilselvi and M. Palaniandavar, *Inorg. Chim. Acta*, 2002, **337**, 420–428.
31 R. Loganathan, S. Ramakrishnan, E. Suresh, A. Riyasdeen, M. A. Akbarsha and M. Palaniandavar, *Inorg. Chem.*, 2012, **51**, 5512–5532.
32 B. Selvakumar, V. Rajendiran, P. Uma Maheswari, H. S. Evans and M. Palaniandavar, *J. Inorg. Biochem.*, 2006, **100**, 316–330.
33 S. Ramakrishnan and M. Palaniandavar, *J. Chem. Soc.*, 2005, **117**, 179–186.
34 S. Ramakrishnan, V. Rajendiran, M. Palaniandavar, V. S. Periasamay, M. A. Akbarsha, B. S. Srinag and H. Krishnamurth, *Inorg. Chem.*, 2009, **48**, 1309–1322.
35 P. Jaividhya, R. Dhivya, M. A. Akbarsha and M. Palaniandavar, *J. Inorg. Biochem.*, 2012, **114**, 94–105.
36 M. Ganesh Pandian, R. Loganathan, S. Ramakrishnan, E. Suresh, A. Riyasdeen, M. A. Akbarsha and M. Palaniandavar, *Polyhedron*, 2013, **52**, 924–938.
37 V. Rajendiran, R. Karthik, M. Palaniandavar, H. S. Evans, V. S. Periasamay, M. A. Akbarsha, B. S. Srinag and H. Krishnamurthy, *Inorg. Chem.*, 2007, **46**, 8208–8221.
38 P. K. Sasmal, S. Saha, R. Majumdar, R. R. Dighe and A. R. Chakravarty, *Inorg. Chem.*, 2010, **49**, 849–859.
39 M. Boiani and M. Gonzalez, *Mini-Rev. Med. Chem.*, 2005, **5**, 409–424.
40 M. E. Reichman, S. A. Rice, C. A. Thomas and P. Poty, *J. Am. Chem. Soc.*, 1954, **76**, 3047–3053.
41 L. A. Ceson and A. R. Day, *J. Org. Chem.*, 1962, **27**, 581–586.
42 M. R. Maurya, A. Kumar, M. Ebel and D. Rehder, *Inorg. Chem.*, 2006, **45**, 5924–5937.
43 G. Kolks, C. R. Frihart, P. K. Coughlin and S. J. Lippard, *Inorg. Chem.*, 1981, **20**, 2933–2940.
44 H. Y. Wu, H. Q. An, B. L. Zhu, S. R. Wang, S. M. Zhang, S. H. Wu and W. P. Huang, *Inorg. Chem. Commun.*, 2007, **10**, 1132–1135.
45 *SMART & SAINT Software Reference manuals, version 5.0*, Bruker AXS Inc., Madison, WI, 1998.
46 G. M. Sheldrick, *SADABS Software for Empirical Absorption Correction*, University of Gottingen, Gottingen, Germany, 2000.
47 *SHELXTL Reference Manuals, version 5.1*, Bruker AXS Inc., Madison, WI, 1998.
48 J. Bernadou, G. Prativiel, F. Bennis, M. Girardet and B. Meunier, *Biochemistry*, 1989, **28**, 7268–7275.
49 M. Blagosklonny and W. S. E1-Diery, *Int. J. Cancer*, 1996, **67**, 386–392.
50 K. Sundaravel, E. Suresh and M. Palaniandavar, *Inorg. Chim. Acta*, 2009, **362**, 199–207.
51 E. C. Constable, C. E. Housecroft, B. M. Kariuki, N. Kelly and C. B. Smith, *C. R. Chim.*, 2002, **5**, 425–430.
52 M. E. Bluhm, M. Ciesielski, H. Gorls, O. Walter and M. Doring, *Inorg. Chem.*, 2003, **42**, 8878.
53 R. Kannappan, S. Tanase, I. Mutikainen, U. Turpeinen and J. Reedijk, *Inorg. Chim. Acta*, 2005, **358**, 383–388.
54 X. Ma, X. Dong, Y. Li and Z. Zhang, *Acta Crystallogr., Sect. E: Struct. Rep. Online*, 2007, **63**, m1729.
55 M. Maurya, C. Haldar, S. Behl, N. Kamatham and F. Avecilla, *J. Coord. Chem.*, 2011, **64**, 2995–3011.
56 M. Maurya, C. Haldar, S. Behl, N. Kamatham and F. Avecilla, *Indian J. Chem., Sect. A: Inorg., Bio-inorg., Phys., Theor. Anal. Chem.*, 2011, **50**, 775–780.
57 M. Balamurugan and M. Palaniandavar, *Inorg. Chem.*, 2001, **40**, 2246–2255.
58 M. Palaniandavar, T. Pandiyan, M. Lakshminarayanan and H. Manoharb, *J. Chem. Soc., Dalton Trans.*, 1995, 455–461.
59 C. J. Oconnor, D. Firmin, A. K. Pant, B. R. Babu and E. D. Stevens, *Inorg. Chem.*, 1986, **25**, 2300–2307.
60 R. J. Majeste, C. L. Klein and E. D. Stevens, *Acta Crystallogr., Sect. C: Cryst. Struct. Commun.*, 1983, **39**, 52–54.
61 A. W. Addison, T. N. Rao, J. Reedijk, J. Van Rjin and G. C. Verschoor, *J. Chem. Soc., Dalton Trans.*, 1984, 1349–1356.
62 Z. Chen, X. Wangb, Y. Li and Z. Guo, *Inorg. Chem. Commun.*, 2008, **11**, 1392–1396.
63 F. Tamboura, M. Gaye, A. Sall, A. Barry and T. Jouini, *Inorg. Chem. Commun.*, 2002, **5**, 235–238.
64 A. Datta, N. Karan, S. Mitra and G. Rosair, *Z. Naturforsch.*, 2002, **57 b**, 999–1002.
65 *Comprehensive Coordination Chemistry*, ed. B. J. Hathaway, G. Wilkinsons, R. G. Gillard and J. A. McCleverty, Pergamon, Oxford, 1987, vol. 5, p. 861.
66 A. W. Addition, Copper coordination chemistry, in *Biohemical and Inorganic Perspectives*, ed. K. D. Karlin and J. Zubieta, Adenine, Guilderland, New York, 1983, p. 109.
67 U. Sakaguchi and A. W. Addison, *J. Chem. Soc., Dalton Trans.*, 1979, 600–608.
68 M. Palaniandavar, I. Somasundaram, M. Lakshminarayanan and H. Manohar, *J. Chem. Soc., Dalton Trans.*, 1996, 1333–1340.
69 M. Murali, M. Palaniandavar and T. Pandiyan, *Inorg. Chim. Acta*, 1994, **224**, 19–25.
70 A. W. Addison, *Inorg. Chim. Acta*, 1989, **162**, 217–220.
71 S. Usha and M. Palaniandavar, *J. Chem. Soc., Dalton Trans.*, 1994, 2277–2283.
72 W. Sakaguchi, *Principles of Nucleic Acid Structure*, Springer, New York, 1983, p. 253.
73 G. S. Manning, *Q. Rev. Biophys.*, 1978, **11**, 179–246.
74 N. Grover, T. W. Welch, T. A. Fairely, M. Cory and H. H. Throp, *Inorg. Chem.*, 1994, **33**, 3544–3548.
75 V. Rajendiran, M. Murali, E. Suresh, S. Sinha, K. Somasundaram and M. Palaniandavar, *Dalton Trans.*, 2008, 2157.
76 A. R. Morgan, J. S. Lee, D. E. Pulleyblank and D. H. Evans, *Nucleic. Acids Res.*, 1979, **7**, 547.
77 L. Li, K. D. Karlin and S. E. Rokita, *J. Am. Chem. Soc.*, 2005, **127**, 520–521.
78 D. S. Sigman, M. D. Kuwabara, C. B. Chen and T. W. Bruice, *Methods Enzymol.*, 1991, **208**, 414–433.
79 A. Amine, Z. Atmani, A. El. Hallaoui, M. Giorgi, M. Pierrotc and M. Réglierc, *Bioorg. Med. Chem. Lett.*, 2002, **12**, 57–60.
80 H. Pezzano and F. Podo, *Chem. Rev.*, 1980, **80**, 365–401.

81 B. Saha, Md. M. Islam, S. Paul, S. Samanta, S. Ray, C. R. Santra, S. R. Choudhury, B. Dey, A. Das, S. Ghosh, S. Mukhopadhyay, G. S. Kumar and P. Karmakar, *J. Phys. Chem. B*, 2010, **114**, 5851–5861.
82 J. A. Simpson, K. H. Cheeseman, S. E. Smith and R. T. Devan, *Biochem. J.*, 1988, **254**, 519–523.
83 M. D. Kuwabara, C. Yoon, T. Goyne, T. Thederahn and D. S. Sigman, *Biochemistry*, 1986, **25**, 7401–7408.
84 M. M. Meijler, O. Zelenko and D. S. Sigman, *J. Am. Chem. Soc.*, 1997, **119**, 1135–1136.
85 C. A. Detmer III, F. V. Pamatong and J. R. Bocarsly, *Inorg. Chem.*, 1996, **35**, 6292–6298.
86 L. O. Rodriguez and S. M. Hecht, *Biochem. Biophys. Res. Commun.*, 1982, **104**, 1470–1476.
87 M. D. Kuwabara, C. Yoon, T. Goyne, T. Thederahn and D. S. Sigman, *Biochemistry*, 1986, **25**, 7401–7408.